Structural characteristics of fat-associated lymphoid tissues and their role in the peritoneal propagation of B-cell lymphoma

Xinkai Jia

PhD student; research assistant

Supervisor: **Dr. Péter Balogh**

University of Pécs, Medical School

Department of Immunology and Biotechnology
Doctoral School of Basic Medical Sciences

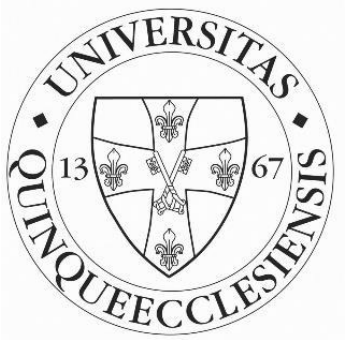

Pécs, 2022

Introduction

Skin and mucosal surfaces are the first protection lines of the mammalian organisms against microbial invasion. When the pathogens pass through these defenses, various immune cells transport them to the neighboring secondary lymphoid organs (1), where leukocytes encounter the pathogens and, as the result, different types of immune reactions are triggered, including the transformation of resting follicles into secondary follicles containing germinal centers (2).

Secondary lymphoid organs, such as the spleen, lymph nodes, and Peyer's patches, develop before birth. Moreover, there is another set of the lymphoid structure which play an important role in mucosal immune defense, including cryptopatches (CPs) and isolated lymphoid follicles (ILFs), which develop after birth (3). In comparison to these well-established lymphoid structures, the role of the serosal compartments in the immune system still remains unknown, even though the serosal surface covering various abdominal organs harbors a large number of B-1 B cells(4).

Although the common understanding of the function of the adipose tissues is energy storage, some research groups have reported that adipose tissue may significantly contribute to the local immune challenges, due to the presence of adipose-associated lymphoid structures (5–7). The typical appearance of these lymphoid structures is less organized, and these are embedded into the adipose tissues collecting various leukocytes by chemokines CXCL1 and CXCl13 (5–8).

The omentum has been considered a policeman in the peritoneal cavity for a long time (9), where milky spots (MSs) are the main contributors to immune surveillance. MSs are highly vascularized tissues containing different types of leukocytes, where B-1 cells produce nature antibodies (10–13). More recently, fat-associated lymphoid clusters (FALCs) were described in the mesenteric fat, which they contain various leukocytes, including Type 2 innate lymphoid cells (ILC2) that play an essential role in B-1 cell proliferation (14, 15).

B cells are one of the most critical factors of adaptive immunity. More specifically, B-1 cells typically secrete natural antibodies, and B-2 cells play roles in regulation, antigen

presentation, and antigen-specific antibody production (16, 17). Besides antigen stimulation, B-cell composition also changes along aging. As the result, age-associated B cells (ABCs) occur which are usually involved in autoantibody production in SLE-prone mice (16–20). Moreover, CD11c positive/T-bet^{high} ABCs can be found outside the typical B-cell compartment in the spleen (21, 22). Due to the phenotypic variants, genotypic characteristics, and clinical courses, it is crucial to study B-cell differentiation and distribution upon antigen activation, as these investigations can also provide understanding B-cell malignancies.

Not only leukocytes, but also various malignant cancer cells, including ovarian cancers, are also able to accumulate in the omental MSs and FALCs after i.p administration of tumor cells or during the metastasis (23–25). Additionally, neutrophil extracellular traps (NETs) have been found in FALC regions at the premetastatic stage of ovarian cancers, which usually reflects a poor prognosis. This indicates extensive interaction among tumor cells, stromal elements, and leukocytes in the process of tumor propagation (26).

In our previous work, we found a mouse spontaneous high-grade B-cell lymphoma (Bc.DLFL1) with restricted in vivo propagation in mesenteric lymph nodes and spleen. In my study, I continued the investigation of the possible binding sites for Bc.DLFL1 and normal B cells on the serosal surface, and cytokine profile alterations of the visceral adipose upon the stress of lymphoma bearing. Furthermore, I have also found a novel type of lymphoid tissues that we termed murine foliate lymphoid aggregates (FALgs), which occur on the various adipose tissues in the abdominal cavity. In addition, I also studied the origin of Bc.DLFL1 cells. In my thesis, I summarize our findings and offer further possible studies for a better understanding of serosal lymphocyte homeostasis and its implications in cancer metastasis.

Aims

Our goals are:

- To investigate the types of adipose-associated lymphoid structures;
- To study Bc.DLFL1 and normal B cells homing process in the peritoneal cavity;
- To investigate Bc.DLFL1 cell characteristics and define its origin;
- To study the microenvironment of fat-associated lymphoid structures following Bc.DLFL1 lymphoma infiltration.

Materials and Methods

1. Mice

8-10 weeks old BALB/c mice and BALB/c^{eGFP} Tg mice were maintained at the specific pathogen-free or minimal disease animal facility of the Department of Immunology and Biotechnology. Prox-1 GFP reporter-transgenic mice were provided by Zoltan Jakus. KiKGR mice (27) were obtained from The Jackson Laboratory. The Bc.DLFL1 lymphoma cells were propagated by i.p. passages of suspension prepared from lymphoma infiltrated mesenteric lymph nodes (28). All procedures involving live animals were conducted in accordance with the guidelines of the Ethics Committee on Animal Experimentation of the University of Pecs.

2. Flow cytometry and sorting

Bc.DLDL1 cells and A20 cells were incubated with fluorochrome-labeled antibodies. For intracellular staining samples were first labeled for cell surface markers, followed by permeabilization, and incubated with mAbs against T-bet and Blimp-1 transcription factors at room temperature. The samples were analyzed using BD FACACalibur and the CellQuest Pro software.

For IgV_H sequencing, Bc.DLFL1 lymphoma cells were purified by Bio-Rad S3e sorter followed by mRNA isolation.

3. Bc.DLFL.1 Ig Vh sequence analysis

Total mRNA from sorted Bc.DLFL1 cells were isolated using NucleoSpin RNA XS kit. cDNA synthesis was performed using the High-Capacity cDNA Reverse Transcription Kit. Endpoint PCR was carried out on Applied Biosystems 2720 Thermal Cycler using DreamTaq TM Green PCR Master Mix. The PCR products were sequenced by a BigDye Terminator Cycle Sequencing Ready Reaction kit v1.1 on an AB 3500 Genetic analyzer and the results were analyzed by the IMGT/HighV-QUEST platform.

4. Whole-mount and tissue section immunohistology and immunofluorescence

For whole-mount immunohistology, the entire gut complex was fixed in 4% paraformaldehyde followed by a short hematoxylin staining, and a selected segment was isolated using stereomicroscopic dissection. The tissue samples were processed with phenylhydrazine hydrochloride followed by saturation with 5% bovine serum albumin (BSA). The samples were incubated with various rat mABs against mouse markers overnight with constant shaking, followed by extensive washing and incubation with HRP-conjugated anti-rat IgG, or fluorochrome-conjugated anti-rat IgG. Confocal fluorescence images were taken using an Olympus FluoView FV1000 laser scanning confocal imaging system. For immunohistochemistry, after adding HRP-conjugated goat anti-rat Ig and development with H_2O_2-Dab, the mounted sections were viewed under an Olympus BX 61 microscope.

For immunohistochemistry of mLN of Bc.DLFL1 lymphoma-bearing mice, frozen sections at 8µm thickness prepared with a Leica CM1850 cryostat were fixed in cold acetone. The sections were incubated with various antibodies at room temperature in a humid chamber. After washing, the sections were incubated with HRP-conjugated anti-rat IgG and developed using diaminobenzidine/H_2O_2 and counter-stained with hematoxylin. For dual immunofluorescence, the sections were incubated with FITC conjugated antibodies and biotinylated mAB visualized with PE-streptavidin.

For combined immunofluorescence of GFP and gp38, the mesentery was fixed, followed by 30% sucrose equilibration overnight. The samples were frozen and 20µm thick cryostat sections were prepared and placed on silanized microscopy slides. After drying, the sections were treated with 5% BSA and incubated with the antibody. Later the samples were mounted with 50% glycerol containing Hoechst-33342. Images were taken using an Olympus Fluoview FV-1000 laser scanning confocal imaging system.

5. Transmission electron microscopy

Dissected mouse intestines and harvested FLAgs were fixed overnight at 4°C with 4% buffered paraformaldehyde, washed in PBS, and postfixed with 2% glutaraldehyde, followed by dehydration in graded ethanol. Tissue samples were treated with 1% osmium tetroxide for

2 h and embedded in a Polybed/Araldite 6500 mixture. The 1µm-thick semithin sections were stained with toluidine blue. The ultrathin sections were contrasted with uranyl acetate and lead citrate, and studied with a Hitachi Electron microscope type H-7600.

6. Cell labeling and transfer

A20 cells and BcDLFL.1 (28) were either labeled with 5mM CFSE, or with 10mM CellTrace Far Red (CTFR) (29). Normal peritoneal B cells were purified from BALB/c mice using MACS separation. For near-infrared (NIR) fluorescence bioimaging, lipophilic XenoLight DiR dye was applied. Following the labeling, the cells were washed and injected into the recipients i.p.

7. NIR fluorescence imaging

MACS-purified B cells or lymphoma cells were labeled with XenoLight DiR dye, followed by an i.p injection. The fluorescence was measured by IVIS Lumina III in vitro imaging system. The tissue binding of Bc.DLFL1 lymphoma cells were quantified in a Bio-One CELLSTAR plate. The data were processed and analyzed using Living Image software.

8. KikGR photoconversion and competitive homing

KikGR lymph nodes were photoconverted at room temperature followed by the mechanical release of lymphocytes (KikR). Unconverted green (KikG) lymph nodes were incubated with mAB MEL-14 (30). The lymphocytes were injected into BALB/c recipients via the tail vein at 1:1 KikG/KikR ratio.

9. BAFF-receptor blockade in lymphoma-bearing mice

BALB/c mice received Bc.DLFL1 cells i.p., followed by 100 µg mBR3-Fc fusion protein treatment i.v. Control mice received a similar dose of irrelevant mouse IgG1 against fluorescein (#F4/1). The experiment was terminated on the 18th day.

10. In vitro culture of Bc.DLFL1 cells and lentivirual transduction with ZsGreen1 Fluoroprotein

Bc.DLFL1 cells were co-cultured with peritoneal exudate cells on 6-well plates with RPMI-1640 and 10% FBS containing 2 mM GlutaMAX and $5x10^{-5}$ M β-mercaptoethanol. VSV-G-pseudotyped lentiviral vectors encoding ZsGreen1 green fluorescent protein driven by EF1α promoter at 20 MOI were incubated with the lymphoma cells overnight. The lymphoma cells were collected, and the highest 10% expression of green fluorescence Bc.DLFL1^{ZsGreen1} cells were sorted using Bio-Rad S3e sorter and cultured in vitro.

11. Homing of blood-borne Bc.DLFL1 ^{ZsGreen1} lymphoma cells

Bc.DLFL1^{ZsGreen} cells were injected i.v, then 12 hours later the spleens from the recipients were processed for immunofluorescence detection using Alexa Fluor 647-labeled anti-B220 and anti-MARCO antibodies.

12. R&D cytokine array of lymphoma tissue extract and quantification

Omentum, mesentery, and mLNs were collected either from the end-stage lymphoma-bearing mice or from untreated BALB/c mice. The tissues were processed with T-PER™ Tissue Protein Extraction Reagent containing protease inhibitor cocktail. The lysate was applied to the membranes from Proteome profiler™ Array Mouse XL Cytokine Array Kit and processed according to the manufacturer's protocol. The membranes were imaged using LAS 4000 image reader and software using chemoluminescence measurements at 180s exposure time and analyzed by ImageJ. A complete clustering method with Euclidean distance was applied to the normalized data set, which was visualized with the pheaetmap function from pheatmap package.

13. Quantitative RT-PCR

Total mRNA from inguinal lymph node, omentum and mesentery homogenates was isolated using NucleoSpin RNA. cDNA was synthesized using a High-Capacity cDNA Reverse Transcription Kit. RT-PCR was run on an Applied Biosystems PRISM 7500 machine in

duplicates using SYBR Green primers for PNAd core proteins and glycosylation enzymes creating the MECA-79 epitope (31).

14. Statistical analysis

Data were analyzed using SPSS 22.0 (IBM). Normality of data distribution was assessed by Shapiro–Wilks test. A *t*-test or Mann– Whitney U test was employed to compare two groups with normally distributed and non-normally distributed data, respectively. Data are represented as mean ± SEM. A p value < 0.05 was considered statistically significant.
Statistical analysis of BAFF-R treatment effect on T/B distribution was performed by student's T-test using GraphPad Prism 5, where significance was considered with p value <0.001. Error bar represents SEM. Kaplan-Meier survival curve was generated by using GraphPad Prism 5 ($p<0.01$).

Results

1. FLAgs as novel forms of serosal lymphoid organoids connected to the mesenteric lymphoid drainage

The high-grade B cell lymphoma Bc.DLFL1 in BALB/c mice shows restricted spreading in the mesenteric lymph nodes and spleen. However, the homing process in early time was not investigated previously. 4 hours after the intraperitoneal injection of DiR dye-labeled lymphoma cells, we found that the omentum exhibits the highest fluorescence signal whereas there are only small foci emitting signals from mesenteric fat, even though the sum of the two sets of signals show no significant difference. Surprisingly, the spleen and the mesenteric lymph nodes are absent of signal emission. With whole-mount immunohistochemistry of CFSE labeled tumor cells and anti-FITC immunodetection, the results display a comparable pattern with NIR imaging. Furthermore, purified B cells exhibit a similar distribution as Bc.DLFL1.

During subsequent microscopic inspections we found leaf-like formations (named foliate lymphoid aggregates - FLAgs) that had bound Bc.DLFL1 cells, which structures were either connected to the mesenteric fat and omental bursa membrane directly, or through a stalk. Similar structures were also present in C57BL/6J mice.

By whole-mount immunohistochemistry, we found intense CD45 expression throughout the whole FLAg, with CD90-positive T-cell region in the center, whereas B220 staining displays a rather even distribution. LYVE-1 positive macrophages sit at the edge of the FLAgs.

With dual immunofluorescence, we confirmed that the T cells concentrate in the center, while B cells distribute in the peripheral regions, which correlates with CCL21 and CXCL13 expression patterns.

Electron microscopic inspection provided a more detailed structure of FLAg composition. We found that the FLAgs are covered with a mesothelial layer. Compressed bulk of lymphocytes presents underneath this cover include plasma cells, together with enriched capillary network and reticular cells. By immunofluorescence we also found fibronectin meshwork throughout the FLAgs and along the stalk. VCAM staining shows intense expression along the stalk and some reticular cells in the FLAgs. FLAgs also contain CD31-positive blood capillaries

containing PNAd positive segments. However, in Prox-1^{GFP} reporter mice, we could only find a few GFP+ cells in the FLAgs. Those results suggested there are no lymphatics in the FLAgs.

2. Normal lymphocyte homing to serosal lymphoid tissues is partly PNAd dependent

We performed a competitive assay by injecting isolated lymphocytes from KikumeGR mice following photoconverison and L-selectin blockade. We found that MEL-14 mAb-pretreated KikG+ cells were dramatically inhibited to enter pLN. Comparing to the pLN, almost 50% reduction has occurred in the mesenteric fat. Quantitative PCR revealed the variable expression of core proteins and glycosylation enzymes for MECA-79-epitope of PNAd which is important for the binding of leukocytes to HEVs. Those data suggested that the migration of blood-borne lymphocytes to serous lymphoid tissues partly depends on L-selectin and PANd binding.

3. Selective homing of BC.DLFL1 from the serosa in the peritoneal cavity through lymphatics

Using CFSE-labeled BC.DLFL1 cells and anti-FITC whole-mount immunohistochemistry, we found lymphoma cells located within mesenteric lymphatic vessels. We also injected CTFR-labeled tumor cells into Prox1^{GFP} mice to verify the intralymphatic accumulation of lymphoma cells. We observed that the lymphoma cells may enter the lymphatic capillaries in the mesentery at early as 4 hours post-injection.

4. Intracellular and cell surface markers of tumor cells indicate the connection between Bc.DLFL1 and ABCs

Earlier findings demonstrated that Bc.DLDL1 cells express CD19, B220, MHC Class II, and MAC-1, lacking CD21 and CD23 as mature B cells marker. Subsequently we found that the lymphoma cells display CCR7 T-cell zone chemokine receptor, and they lack CXCR5 guiding lymphocytes to the follicles. Later we also demonstrated that the majority of the Bc.DLFL1 cells are CXCR4 positive, which has been reported as a marker of a minor pool termed CD11c+ age-associated B cells (ABCs) (20). Sequentially, we also discovered that

Bc.DLFL.1 also expresses a high level of CD11c. The CD11c-positive ABC subset also typically produces the T-bet transcription factor (18, 20, 32). We could confirm that Bc.DLFL1 cells displayed T-bet and Blimp-1. However, the cells were negative for plasma cell marker CD138, and positive for the activation markers CD80 and CD86.

Moreover, the V_H region of lymphoma cells contains 11 non-silent mutations and 1 silent mutation. Additionally, anti-mouse IgG2a isotype-specific detection revealed strong cytoplasmic staining, indicating a heavy chain isotype switch.

All those data suggest that Bc.DLFL1 lymphoma originate from ABCs, whereas the production of Blimp-1 and IgG2a isotype together with the lack of CD138 points to memory plasmablast derivation.

5. Bc.DLFL1 cells concentrate in the extrafollicular region of the spleen

Previous data suggested extrafollicular homing preference for Bc.DLFL1 cells. To trace the lymphoma cells, we have developed Bc.DLFL1^{ZsGreen} cells. 12 hours after i.v injection of Bc.DLFL1^{ZsGreen} cells, we found that most of the green cells in the spleen are at the extrafollicular parts of the white pulp and in the marginal zone.

6. BAFF-R blockade prolongs the survival of lymphoma bearing mice survival

BAFF plays a critical role in mature B cell survival; therefore, we tested the activity of BAFF-R and its analogues BCMA and TACI on the lymphoma cells. The results showed that Bc.DLFL1 expresses a high level of BAFF-R and TACI compared to normal B cells, whereas there was no difference in BCMA expression level.

We further tested the function of BAFF-R in the disease progression by i.v injecting mBR3-Fc which is a soluble BAFF-R decoy receptor, into lymphoma-seeded mice on days 1,4,6,8 post lymphoma administration. In comparison, a control group of mice received normal mouse IgG1. By the 18th day, the majority of mice in the experimental group were alive, whereas in the control group the majority had succumbed. These data suggest the mBR-3Fc treatment will efficiently prolong the survival of the mice bearing lymphoma.

7. Alterations of stroma elements and tissue-specific cytokine landscape

By anti-B220 and Ki-67 immunohistochemistry we confirmed that the mesenteric and omental fat had become thickened and brittle in mice at the advanced stage of the tumor, indicating the substantial replacement of adipose tissue with lymphoma infiltrate. By using eGFP transgenic mice, we found a network of gp38+/eGFP+ fibroblastic reticular cells (FRCs) at the edge of the bulk of the lymphoma in the mesentery at advanced stage of lymphoma. In control mesentery, the gp38 positive fibroblastic cells typicallly appear in the perivascular area. In addition, by comparing the cytokine profile of mesenteric lymph nodes, omentum, and mesenteric fat from lymphoma-bearing mice and control mice, we found significant differences between the various lymphoma-laden tissues and between their normal counterparts as well, indicating that the presence of lymphoma alters in a tissue-specific manner the local cytokine landscape.

New findings of my PhD research

1. We have identified murine FLAgs (foliate lymphoid aggregates) as novel forms of serosa-associated lymphoid organs with partly compartmentalized lymphoid structure, composed of a FLAg body and stalk connecting to the bursal peritoneum or the omental and mesenteric adipose tissue;
2. We have demonstrated that the entry of B cells and Bc.DLFL1 high-grade B-cell lymphoma cells from the peritoneal cavity to FLAgs involves LYVE-1-positive macrophages, whereas the homing of blood-borne lymphocytes is partly L-selectin dependent;
3. We have established that various B-cell lymphoma cells compartmentalize within FLAgs according to their chemokine receptor expression pattern, with CCR7 guiding Bc.DLFL1 lymphoma cells into the central region producing CCL21, and CXCR5 guiding A20 lymphoma cells to the peripheral rim of FLAg body containing CXCL13, respectively;
4. We have identified the mesenteric lymphatics as exit routes for the intraperitoneally injected B lymphocytes;
5. We have established that the FLAg body is arranged around VCAM-1–positive fibroblastic cells, and it contains an extensive CD31-positive vasculature;
6. We have defined Bc.DLFL1 lymphoma cells as age-associated B-cell (ABC) derived plasmablastic lymphoma, expressing T-bet, CD11c and CXCR4 which, together with CCR7, directs their positioning to the splenic T-cell zone, marginal zone and red pulp, respectively;
7. We have established that the inhibition of BAFF-R ligand binding significantly promotes the survival of lymphoma-bearing recipient mice;
8. We have demonstrated that the adipose expansion of Bc.DLFL1 lymphoma cells alters the cytokine landscape in a tissue-specific manner, and causes expansion of gp38-positive fibroblastic reticular cells.

References

1. Cornes, J. S. 1965. Number, size, and distribution of Peyer's patches in the human small intestine: Part I The development of Peyer's patches. *Gut* 6: 225–229.
2. Liu, X., Y. Zhao, and H. Qi. 2022. T-independent antigen induces humoral memory through germinal centers. *J. Exp. Med.* 219.
3. McDonald, K. G., J. S. McDonough, B. K. Dieckgraefe, and R. D. Newberry. 2010. Dendritic Cells Produce CXCL13 and Participate in the Development of Murine Small Intestine Lymphoid Tissues. *Am. J. Pathol.* 176: 2367–2377.
4. Ansel, K. M., R. B. S. Harris, and J. G. Cyster. 2002. CXCL13 Is Required for B1 Cell Homing, Natural Antibody Production, and Body Cavity Immunity. *Immunity* 16: 67–76.
5. Meza-Perez, S., and T. D. Randall. 2017. Immunological Functions of the Omentum. *Trends Immunol.* 38: 526–536.
6. Cruz-Migoni, S., and J. Caamaño. 2016. Fat-associated lymphoid clusters in inflammation and immunity. *Front. Immunol.* 7.
7. Jackson-Jones, L. H., P. Smith, J. R. Portman, M. S. Magalhaes, K. J. Mylonas, M. M. Vermeren, M. Nixon, B. E. P. Henderson, R. Dobie, S. Vermeren, L. Denby, N. C. Henderson, D. J. Mole, and C. Bénézech. 2020. Stromal Cells Covering Omental Fat-Associated Lymphoid Clusters Trigger Formation of Neutrophil Aggregates to Capture Peritoneal Contaminants. *Immunity* 52: 700-715.e6.
8. Bénézech, C., E. Mader, G. Desanti, M. Khan, K. Nakamura, A. White, C. F. Ware, G. Anderson, and J. H. Caamaño. 2012. Lymphotoxin-β Receptor Signaling through NF-κB2-RelB Pathway Reprograms Adipocyte Precursors as Lymph Node Stromal Cells. *Immunity* 37: 721–734.
9. Hall, J. C., K. A. Heel, J. M. Papadimitriou, and C. Platell. 1998. The pathobiology of peritonitis. *Gastroenterology* 114: 185–196.
10. Fedorko, M. E., and J. G. Hirsch. 1971. Studies on transport of macromolecules and small particles across mesothelial cells of the mouse omentum: I. Morphologic aspects. *Exp. Cell Res.* 69: 113–127.
11. Gerber, S. A., V. Y. Rybalko, C. E. Bigelow, A. A. Lugade, T. H. Foster, J. G. Frelinger, and E. M. Lord. 2006. Preferential attachment of peritoneal tumor metastases to omental immune aggregates and possible role of a unique vascular microenvironment in metastatic survival and growth. *Am. J. Pathol.* 169: 1739–1752.
12. Hodel, C. 1970. Ultrastructural studies on the absorption of protein markers by the greater omentum. *Eur. Surg. Res.* 2: 435–449.
13. Avrameas, S., and T. Ternynck. 1995. Natural autoantibodies: The other side of the immune system. *Res. Immunol.* 146: 235–248.
14. Bénézech, C., N. T. Luu, J. A. Walker, A. A. Kruglov, Y. Loo, K. Nakamura, Y. Zhang, S. Nayar, L. H. Jones, A. Flores-Langarica, A. McIntosh, J. Marshall, F. Barone, G. Besra, K. Miles, J. E. Allen, M. Gray, G. Kollias, A. F. Cunningham, D. R. Withers, K. M. Toellner, N. D. Jones, M. Veldhoen, S. A. Nedospasov, A. N. J. McKenzie, and J. H. Caamaño. 2015. Inflammation-induced formation of fat-associated lymphoid clusters. *Nat. Immunol.* 16: 819–828.
15. Moro, K., T. Yamada, M. Tanabe, T. Takeuchi, T. Ikawa, H. Kawamoto, J. I. Furusawa, M. Ohtani, H. Fujii, and S. Koyasu. 2010. Innate production of TH 2 cytokines by adipose tissue-associated c-Kit+ Sca-1+ lymphoid cells. *Nature* 463: 540–544.
16. Kugler-Umana, O., P. Devarajan, and S. L. Swain. 2020. Understanding the Heterogeneous Population of Age-Associated B Cells and Their Contributions to Autoimmunity and Immune Response to Pathogens. *Crit. Rev. Immunol.* 40: 297–309.
17. Baba, Y., Y. Saito, and Y. Kotetsu. 2020. Heterogeneous subsets of B-lineage regulatory cells (Breg cells). *Int. Immunol.* 32: 155–162.
18. Hao, Y., P. O'Neill, M. S. Naradikian, J. L. Scholz, and M. P. Cancro. 2011. A B-cell subset uniquely responsive to innate stimuli accumulates in aged mice. *Blood* 118: 1294–1304.
19. Rubtsov, A. V., K. Rubtsova, A. Fischer, R. T. Meehan, J. Z. Gillis, J. W. Kappler, and P. Marrack. 2011. Toll-like receptor 7 (TLR7)-driven accumulation of a novel CD11c+ B-cell population is important for the development of autoimmunity. *Blood* 118: 1305–1315.
20. Cancro, M. P. 2020. Age-Associated B Cells. *Annu. Rev. Immunol.* 38: 315–340.
21. Rubtsov, A. V., K. Rubtsova, J. W. Kappler, J. Jacobelli, R. S. Friedman, and P. Marrack. 2015. CD11c-Expressing B Cells Are Located at the T Cell/B Cell Border in Spleen and Are Potent APCs. *J. Immunol.* 195: 71–79.
22. Johnson, J. L., R. L. Rosenthal, J. J. Knox, A. Myles, M. S. Naradikian, J. Madej, M. Kostiv, A. M. Rosenfeld, W. Meng, S. R. Christensen, S. E. Hensley, J. Yewdell, D. H. Canaday, J. Zhu, A. B. McDermott, Y. Dori, M. Itkin, E. J. Wherry, N. Pardi, D. Weissman, A. Naji, E. T. L. Prak, M. R. Betts, and M. P. Cancro. 2020. The Transcription Factor T-bet Resolves Memory B Cell Subsets with Distinct Tissue Distributions and Antibody Specificities in Mice and Humans. *Immunity* 52: 842-855.e6.
23. Clark, R., V. Krishnan, M. Schoof, I. Rodriguez, B. Theriault, M. Chekmareva, and C. Rinker-Schaeffer. 2013. Milky spots promote ovarian cancer metastatic colonization of peritoneal adipose in experimental models. *Am. J. Pathol.* 183: 576–591.
24. Liu, J., X. Geng, and Y. Li. 2016. Milky spots: omental functional units and hotbeds for peritoneal cancer metastasis. *Tumor Biol.* 37: 5715–5726.
25. Kasagi, Y., Y. Harada, Y. Morodomi, T. Iwai, S. Saito, K. Yoshida, E. Oki, H. Saeki, K. Ohgaki, M. Sugiyama, M. Onimaru, Y. Maehara, and Y. Yonemitsu. 2016. Peritoneal dissemination requires an Sp1-dependent CXCR4/CXCL12 signaling axis and extracellular matrix-directed spheroid formation. *Cancer Res.* 76: 347–357.
26. Lee, W. J., S. Y. Ko, M. S. Mohamed, H. A. Kenny, E. Lengyel, and H. Naora. 2019. Neutrophils facilitate ovarian cancer premetastatic niche formation in the omentum. *J. Exp. Med.* 216: 176–194.
27. Nowotschin, S., and A. K. Hadjantonakis. 2009. Use of KikGR a photoconvertible green-to-red fluorescent protein for cell labeling and lineage analysis in ES cells and mouse embryos. *BMC Dev. Biol.* 9.
28. Vojkovics, D., Z. Kellermayer, D. Heidt, M. Mihalj, B. Kajtár, D. Ernszt, T. Kovács, P. Németh, and P. Balogh. 2016. Isolation and Characterization of a Murine Spontaneous High-Grade Follicular Lymphoma with Restricted In Vivo Spreading – a Model for Lymphatic Metastasis Via the Mesentery. *Pathol. Oncol. Res.* 22: 421–430.
29. Zhou, W., H. C. Kang, M. O'Grady, K. M. Chambers, B. Dubbels, P. Melquist, and K. R. Gee. 2016. CellTrace™ Far Red & CellTracker™ Deep Red. *J. Biol. Methods* 3: e38.
30. Chin, S. S., L. Chorro, J. Chan, and G. Lauvau. 2019. Splenic innate B1 B cell plasmablasts produce sustained granulocyte-macrophage colony-stimulating factor and interleukin-3 cytokines during murine malaria infections. *Infect. Immun.* 87.
31. Czömpöly, T., Á. Lábadi, Z. Kellermayer, K. Olasz, H.-H. Arnold, and P. Balogh. 2011. Transcription Factor Nkx2-3 Controls the Vascular Identity and Lymphocyte Homing in the Spleen. *J. Immunol.* 186: 6981–6989.
32. Rubtsova, K., A. V. Rubtsov, J. M. Thurman, J. M. Mennona, J. W. Kappler, and P. Marrack. 2017. B cells expressing the transcription factor T-bet drive lupus-like autoimmunity. *J. Clin. Invest.* 127: 1392–1404.

List of publications

My doctoral thesis is based on the following publications:

Jia X, Gábris F, Jacobsen Ó, Bedics G, Botz B, Helyes Z, Kellermayer Z, Vojkovics D, Berta G, Nagy N, Jakus Z, Balogh P. Foliate Lymphoid Aggregates as Novel Forms of Serous Lymphocyte Entry Sites of Peritoneal B Cells and High-Grade B Cell Lymphomas. J Immunol. 2020 204:23-36.* (IF: 5,422)

Jia X, Berta G, Gábris F, Kellermayer Z, Balogh P. Role of adipose-associated lymphoid tissues in the immunological homeostasis of the serosal surface. Immunol Lett. 2020 228:135-141. (IF: 3,685)

Jia X, Bene J, Balázs N, Szabó K, Berta G, Herczeg R, Gyenesei A, Balogh P.. Age-Associated B Cell Features of the Murine High-Grade B Cell Lymphoma Bc.DLFL1 and Its Extranodal Expansion in Abdominal Adipose Tissues. J Immunol. 2022 208:2866-2876. doi:10.4049/jimmunol.2100956. ** (IF: 5,422)

Other publications related to this work:

Ritter Z, Zámbó K, Jia X, Szöllősi D, Dezső D, Alizadeh H, Horváth I, Hegedűs N, Tuch D, Vyas K, Balogh P, Máthé D, Schmidt E. Intraperitoneal Glucose Transport to Micrometastasis: A Multimodal In Vivo Imaging Investigation in a Mouse Lymphoma Model. Int J Mol Sci. 2021 22:4431. (IF: 5,923)

Ritter Z, Zámbó K, Balogh P, Szöllősi D, Jia X, Balázs Á, Taba G, Dezső D, Horváth I, Alizadeh H, Tuch D, Vyas K, Hegedűs N, Kovács T, Szigeti K, Máthé D, Schmidt E. In situ lymphoma imaging in a spontaneous mouse model using the Cerenkov Luminescence of F-18 and Ga-67 isotopes. Sci Rep. 2021 11:24002. (IF: 4,379)

Other Publications

Khanfar E, Olasz K, Gajdócsi E, Jia X, Berki T, Balogh P, Boldizsár F. Splenectomy modulates the immune response but does not prevent joint inflammation in a mouse model of RA [published online ahead of print, 2022 May 16]. Clin Exp Immunol. 2022;uxac052. doi:10.1093/cei/uxac052 (IF: 5,732)

*Included in Top Reads (https://www.jimmunol.org/content/204/1/1)

**The cover of the June 15, 2022 issue of The JI

Acknowledgments

I would like to say thank you to all the people who have appeared in my life who made me become who I am, and especially to those who have encouraged me to pursue my dream.

I would like to express my gratitude to my supervisor Dr. Péter Balogh who has been supporting my staying here and guiding me throughout the whole duration of my Ph.D. study.

Special thanks to Dr. Zoltán Kellermayer and Dr. Fanni Gábris for some technical and experimental advice.

Many thanks to Dr Gergely Berta for confocal microscopic images, and to Dr. Róbert Herczeg to Dr. Attila Gyenesei for generating the heat map and data analysis.

I am genuinely grateful to all my colleagues at the Department of Immunology and Biotechnology.

I thank my family who supports me by letting me go and respects my decisions.